Microwave selective heating of electric arc furnace dust constituents toward sustainable recycling: contribution of electric and magnetic fields

Sanad Altarawneh,[1,*] Mohammad Al-Harahsheh,[2] Adam Buttress,[1] Chris Dodds,[1] Jose Rodriguez,[1] Sam Kingman,[1]

[1] Faculty of Engineering, University of Nottingham, Nottingham, NG7 2RD, UK

[2] Chemical Engineering Department, Jordan University of Science and Technology, Irbid, 22110, Jordan

Abstract

Microwave heating of waste electric arc furnace dust (EAFD) for the purpose of its remediation has been studied extensively. However, these studies considered EAFD as a bulk material without addressing either the relative response of its individual constituents or the specific interactions with either the electric or magnetic fields of an electromagnetic wave. In this work, we present a study of the relative contribution of the electromagnetic wave components to the heating of EAFD constituents using separated electric and magnetic microwave fields. ZnO, $ZnFe_2O_4$, Fe_3O_4, and graphite were found to be the main contributors to the heating of EAFD based on their dielectric properties and heating profiles. ZnO and $ZnFe_2O_4$ heated only in the electric field yielding temperatures of 846 and 720 °C after heating for 30 and 40 s, respectively at a power input of 118 ± 12 W. Fe_3O_4 and graphite, in contrast, heated in both electric and magnetic fields owing to their respective magnetic and conductive nature. It is suggested that the selective magnetic heating of Fe_3O_4 has significant implications for the selective extraction of zinc and lead through thermal treatment of EAFD with halogenated plastics such as polyvinyl chloride (PVC).

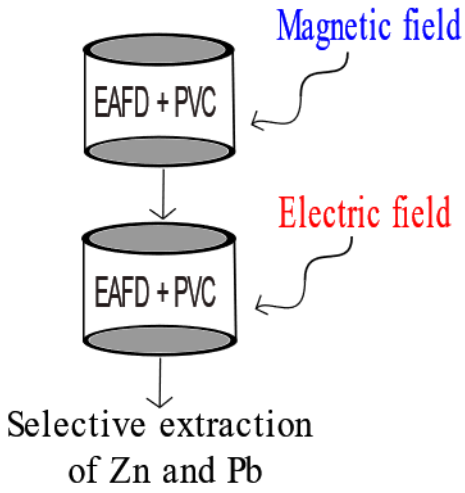

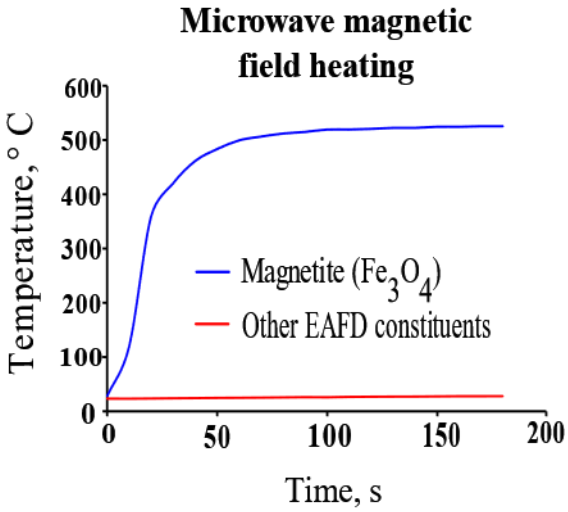

Keywords: EAFD, Metal extraction, Dielectric properties, Magnetic hysteresis, Magnetite

*corresponding author

Tel.: +447979038915

E-mail address: sanad.altarawneh@nottingham.ac.uk

E-mail addresses of authors:

Mohammad Al-Harahsheh: msalharahsheh@just.edu.jo

Adam Buttress: ezzajb@exmail.nottingham.ac.uk

Chris Dodds: enzcjd@exmail.nottingham.ac.uk

Jose Rodriguez: ezzjr1@exmail.nottingham.ac.uk

Sam Kingman: enzsk@exmail.nottingham.ac.uk

1 Introduction

Steel manufacturing is strongly linked to the economic development and growth [1]. The amount of crude steel produced globally per year in 1950 was 189 Mt, which increased to 850 Mt in 2000 and up to 1809 Mt in 2018; the share of electric arc furnaces (EAFs) amounts to 28% of the total production in 2018 [1]. During steel manufacturing, hazardous EAFD is generated in large amounts [2]. According to estimations, 15-20 kg of EAFD is emitted for every ton of recycled steel [3]. Most of the charge supplied to EAFs is steel scrap [4], and since most of the recycled steel is galvanised, high zinc concentrations are generally found in EAFD [5-8]. The high zinc content and the large accumulation rate render EAFD an attractive secondary source for zinc. Methods used for the utilisation of EAFD as a zinc source can be categorised into hydrometallurgical and pyrometallurgical [2]. While the hydrometallurgical methods are less energy intensive and more environmentally sound, this approach suffers from incomplete metallic extraction, harshness of the leaching medium, and the contamination of the leaching solutions with undesired metallic species [3, 9-12]. The pyrometallurgical approach, on the other hand, has found wider commercial application. The Waelz process, for instance, is the most commonly applied pyrometallurgical method for the treatment of EAFD [13]. According to estimates, 80% of the recycled dust is treated in the Waelz kiln [14]. In this kiln, EAFD is exposed to a high temperature carbothermic reduction where zinc is selectively volatilised, oxidised, and finally collected as ZnO. More recently, however, attention has been directed towards the thermal treatment of EAFD with halogenated plastics such as polyvinyl chloride (PVC) and tetrabromobisphenol A (TBBPA) [2, 8, 15-20]. In these studies, EAFD is reacted with the halogen acids generated from these plastics when heated up to temperatures of 200 – 300 °C, followed by water leaching of the resulting metal

halides [8, 16]. A problem encountered in this approach, is the reaction of Fe_3O_4 in EAFD with the halogen acids, leading to the formation of iron chloride/bromide, which is carried over to the final leaching solution as Fe^{2+} and impairs the extraction of zinc at a high purity [16, 17, 21]. Since these techniques require significant heat addition, much work has been directed towards studying the use of microwave energy as a heating source for the treatment of EAFD [16, 17, 22-27]. Ye et al. [27, 28] reported the possibility of using microwaves for the carbothermic reduction of EAFD with biochar and identified the main heating mechanisms for the system. Zhou et al. [23] and Omran et al. [25] studied the microwave-assisted reduction of EAFD using graphite as a reducing agent, while Sun et al. [22] reported the effect of different carbon types for the reduction of EAFD. Al-Harahsheh et al. [16, 17], measured the dielectric properties of EAFD and pyrolysed it with halogenated plastics for metal extraction using microwave energy as the heating source. In these studies, only the bulk temperature rise was considered when EAFD was microwave treated as a whole. The contribution of the individual component phases to the bulk temperature rise was not identified. The detailed knowledge of the relative response of each mineral phase to microwave energy can significantly improve the understanding of the underpinning mechanism of microwave-assisted recycling of EAFD. The presence of magnetic and electrically conductive species in EAFD has been reported in the literature [21, 29, 30]. Magnetite (Fe_3O_4), a well-known iron bearing magnetic mineral, was reported in many studies to be present in appreciable amounts in EAFD [6, 21, 31, 32]. Al-Harahsheh [21], reported that Fe_3O_4 is present at a mass percentage of 10.4%, which in turn suggests that a different response of EAFD should be observed when placed in either magnetic or electric field components of a microwave cavity. In this work we seek to

understand this fundamental concept, whereby microwaves are applied to high purity EAFD constituents in separated electric and magnetic microwave fields with a power input of 118 ± 12 W. Dielectric characterisation of the individual mineral phases was undertaken. These properties were input into an electromagnetic model (COMSOL Multiphysics) of the microwave heating system, to enable the system to be adjusted so the interaction of the minerals with either the magnetic or electric field component could be controlled.

The implication of the current work for the selective extraction of zinc and lead from EAFD through the thermal treatment with halogenated plastics was also assessed based on a previously conducted thermodynamics analysis by Al-Harahsheh [19, 21].

2 Microwave-matter interaction

2.1 Heating mechanisms

An electromagnetic wave can best be visualised in the form of a dual sinusoidal function carrying both electric and magnetic fields as seen in Figure 1.

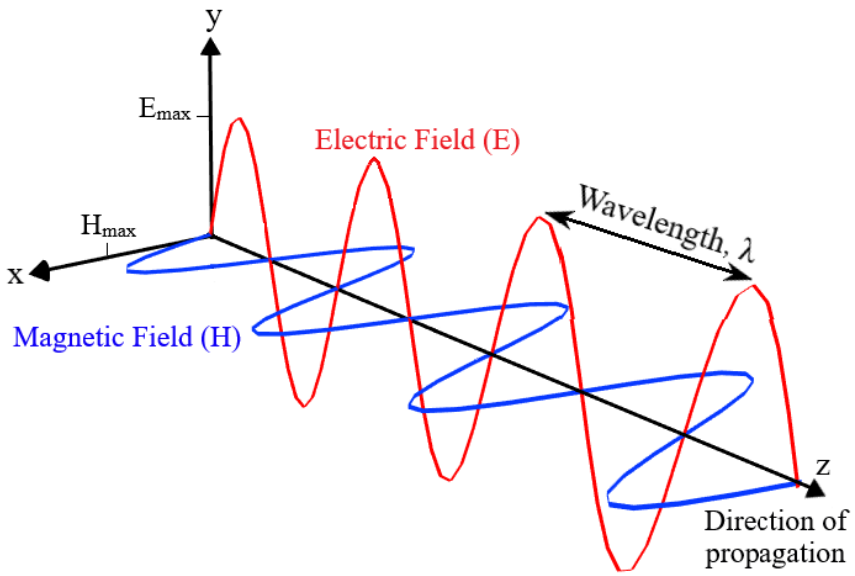

Figure 1. A schematic representation of a travelling electromagnetic wave.

The interaction of a material with microwaves causes either the electric or magnetic fields to be disturbed which ultimately depends on the nature of the material. Thus, the heating action of microwaves can be attributed to dielectric, magnetic, and conductive losses [33].

2.1.1 Dipolar polarisation loss

Materials with permanent molecular dipoles heat by the dipolar polarisation mechanism due to their interaction with the electric field component of microwaves [34]. Quantitatively, the material's response to the electric field is usually represented by the dielectric constant (ε′) and the loss factor (ε′′) of the material. The former represents the ability of the material to store energy as charge polarisation, while the latter represents the

ability of the material to dissipate this energy as heat [34-36]. Both are expressed in terms of the complex dielectric constant (ε) as follows [37]:

$$\varepsilon = \varepsilon' - j\,\varepsilon'' \quad (1)$$

Where $j = \sqrt{-1}$. The power dissipated in the material as heat shows a direct dependency on the imaginary part of the complex dielectric constant of the material [38]:

$$\text{Power} = \omega.\varepsilon''.\varepsilon_o\, E^2{}_{rms} \quad (2)$$

Where ω is the angular frequency of microwaves, ε_o is the permittivity of free space, E_{rms} is the root mean square of the intensity of the microwave electric field.

2.1.2 Magnetic hysteresis loss

Similar to dielectrics, an external alternating magnetic field interacts with the magnetic dipoles present in magnetic materials which makes them oscillate as well [39]. Since the domains in magnetic materials become permanently magnetised in a certain direction [40], a magnetic field in the opposite direction is needed in order to demagnetise and eventually magnetise in the opposite direction, forming a magnetisation hysteresis loop. The amount of energy dissipated in the material is directly related to the area enclosed in the hysteresis loop [41]. Likewise, a complex magnetic permeability can be defined for magnetic materials [42]:

$$\mu = \mu' - j\,\mu'' \quad (3)$$

Where μ' is a measure of the ability of the material to store magnetic energy in the form of magnetisation (magnetic polarisation) and μ'' is its ability to dissipate this energy as heat.

The power dissipated in the magnetic field is primarily related to the imaginary part of permeability as follows [38]:

$$\text{Power} = \omega . \mu'' . \mu_o \, H^2{}_{rms} \quad (4)$$

Where μ_o is the permeability of free space and H_{rms} is the root mean square of the intensity of the microwave magnetic field.

2.1.3 Electric field conductive loss

Translational motion of charge in the form of electrons or ions also contribute significantly to microwave heating. When a conductive material is exposed to microwaves, the electric field drives the free charge through the material resulting in resistive heating [42-45]. The conduction loss factor and the power dissipated per unit volume of the material are given by:

$$\varepsilon''_{conduction} = \frac{\sigma}{\omega \varepsilon_o} \quad (5)$$

$$\text{Power} = \sigma . E^2{}_{rms} \quad (6)$$

Where σ is the electrical conductivity of the material.

2.1.4 Magnetic field conductive loss

The alternating nature of the magnetic field in microwaves produces an electromotive force (emf) in conductive materials (Faraday's law). This emf pushes an electric current through the material resulting in resistive heating. If the material is solid and not hollow, densely packed currents form which are referred to as eddy currents. The power dissipated in a conductive solid disc due to eddy currents is given as [46]:

$$\text{Power} = \frac{\pi}{256} D^4 . h . \frac{B_0^2 \omega^2}{\rho} \quad (7)$$

Where D is the diameter of the disc, h is the disc thickness, B_o is the intensity of the magnetic flux, and ρ is the electrical resistivity of the material.

3 Experimental work

3.1 Materials

All materials used in this work were of high purity. ZnO, Fe_2O_3, PbO, C, and $CaCO_3$ were purchased from Fisher Scientific with purities > 99.99% except for $CaCO_3$ which was at 99.95%. Fe_3O_4 and SiO_2, were purchased from Sigma-Aldrich with purities of 99.99 and 99.995%, respectively. Finally, $ZnFe_2O_4$ was purchased from Alpha Aesar with a purity ≥ 99%.

3.2 Cavity perturbation measurements

The cavity perturbation technique was used for measuring the dielectric properties [42, 47]. A schematic diagram of the apparatus is presented in Figure 2.

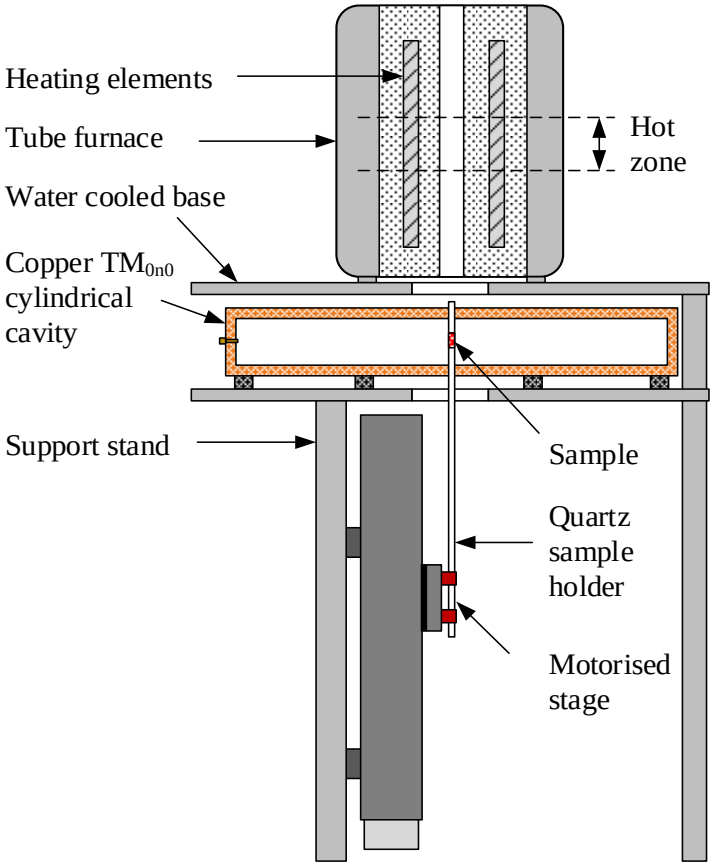

Figure 2. Schematic diagram of the cavity perturbation apparatus.

A quartz sample holder with an internal diameter of 4 mm was used. Before measuring the properties of the powders, the effect of the empty tube was first measured and subtracted later. A specified mass of powder sample was loaded inside the tube and was packed to a specific height, so that samples with similar bulk density can be reproduced. The sample holder was then mounted on a motorised stage which elevates the sample to an electrically controlled furnace to adjust the temperature of the sample (Figure 2). Once the desired temperature was reached, the sample was held at that temperature for 8 – 10 min, to ensure homogeneity of the temperature inside the sample. The motorised stage then immediately lowers the sample into the cylindrical copper cavity, where the dielectric properties of the sample are derived from the change in the resonance frequency and the quality factor (with and without the sample). Measurements were performed in the temperature range of 25 –

1100 °C at frequencies of 2.47 GHz and 912/910 MHz. Dielectric properties extracted at 2.47 GHz were important for understanding the heating behaviour and for the building of the electromagnetic simulation of the heating setup. Moreover, these frequencies were used since they fall within the range of the allocated frequency bands for Industrial, Scientific, and Medical purposes (ISM). Materials that were prone to oxidation such as Fe_3O_4 were purged through the lower portion of the quartz sample holder with 99.9992 % pure N_2 at ~ 10 mL/min. Since N_2 gas contains trace amounts of O_2, it was initially passed through a sacrificial Fe_3O_4 sample which scrubbed the purging gas completely from O_2 traces. Powders were analysed using X-Ray Diffraction (XRD) technique before and after the measurements.

3.3 Microwave electric and magnetic field heating

3.3.1 Rectangular waveguide and TE_{10} cavity

A straight aluminium rectangular waveguide connected to a TE_{10} cavity with a height and width of 43 and 86 mm was used for the heating trials. A schematic diagram of the setup is shown in Figure 3.

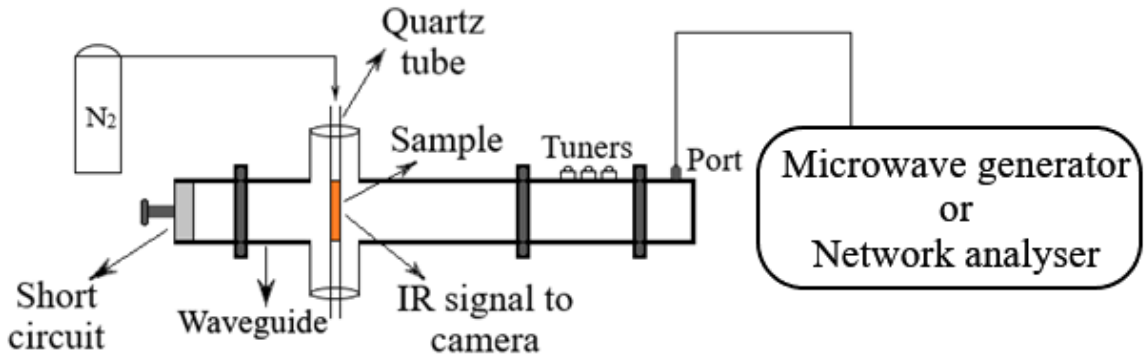

Figure 3. Schematic diagram of the experimental setup for the electric and magnetic heating.

In a TE_{10} cavity, the microwave electric field is polarised parallel to the height of the sample (Figure 4), while the magnetic field rotates in circles around the electric field. The distribution of the microwave fields inside the cavity is presented in Figure 4 in the form of green lines.

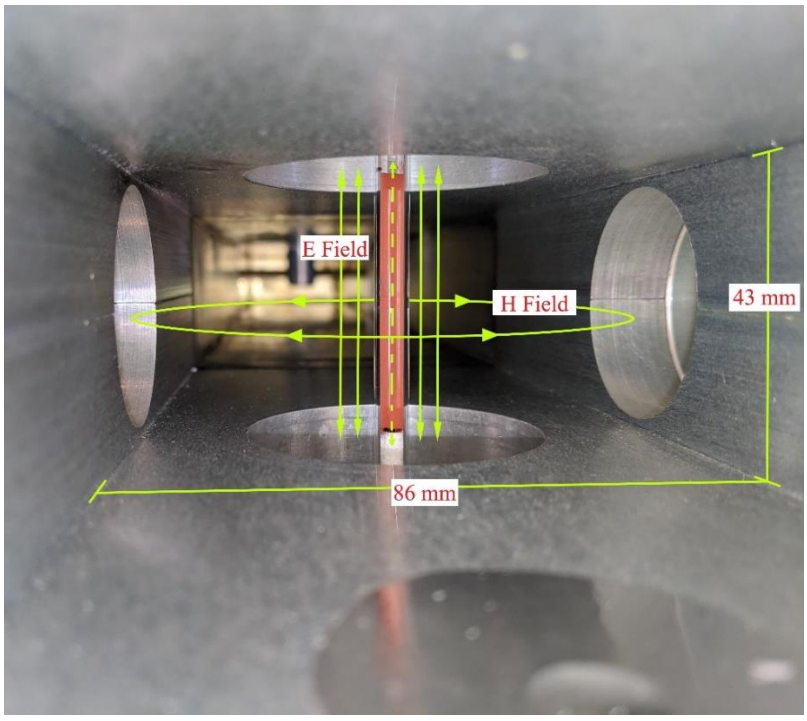

Figure 4. Vertical positioning of hematite (Fe_2O_3) sample inside a TE_{10} cavity; green lines show the distribution of the electric (E) and magnetic (H) fields.

In the case shown in Figure 4, the electric field passes through the sample, while the magnetic field does not, and hence, electric field interaction with the sample is at a maximum. As the short circuit is moved away from the sample (Figure 3), the circular magnetic field lines will start passing through the sample, penetrating it from the side at an angle of 90°, with the electric field shifted away. At this point, heating via the magnetic component of the microwaves dominates.

3.3.2 Sample size consideration and heating procedure

Samples were loaded in powder form in a quartz tube with an internal diameter of 4 mm as shown in Figure 4. Since the maximum intensities of the electric and magnetic fields for a 2.47 GHz standing guided wave are theoretically separated by a distance of ~ 43 mm, using a small sample size was crucial to reduce the interference between the electric and the magnetic fields (i.e., to expose the sample to one field at a time). The quartz tube was vertically fixed through the chokes by means of guide bungs which allowed accurate positioning of the sample through the centre of the cavity at an angle of 90° with respect to horizontal.

An electromagnetic model of the heating setup was constructed on COMSOL Multiphysics, based on the measured dimensions of the cavity to confirm the positions of the electric and magnetic fields within the waveguide. The position of the short circuit in the model was adjusted until it gave either maximum electric or magnetic field within the sample. To confirm the reliability of the model, a vector network analyser (Agilent E5071C) was connected from the port side (Figure 3) to measure the degree of power absorption in each case. For the heating tests, a microwave generator (SAIREM Miniflow 200SS) was connected through a N-Type port using a coaxial transmission line. The power deposited into the waveguide during the heating tests was 118 ± 12 W at a frequency of 2.47 GHz. Through the observation port (left hole in Figure 4), a thermal Infra-Red camera (NEC Avio H2640) was used to measure the surface temperature of the sample with the emissivity set at 0.75. Samples that are prone to oxidation (graphite and Fe_3O_4) were purged with 99.9992% pure N_2 for at least 10 min., after which the flow was shut off and heating was started.

3.3.3 Electromagnetic simulation

Figure 5 shows the components of the heating setup on COMSOL Multiphysics software and the distribution of the electric and magnetic fields inside the waveguide.

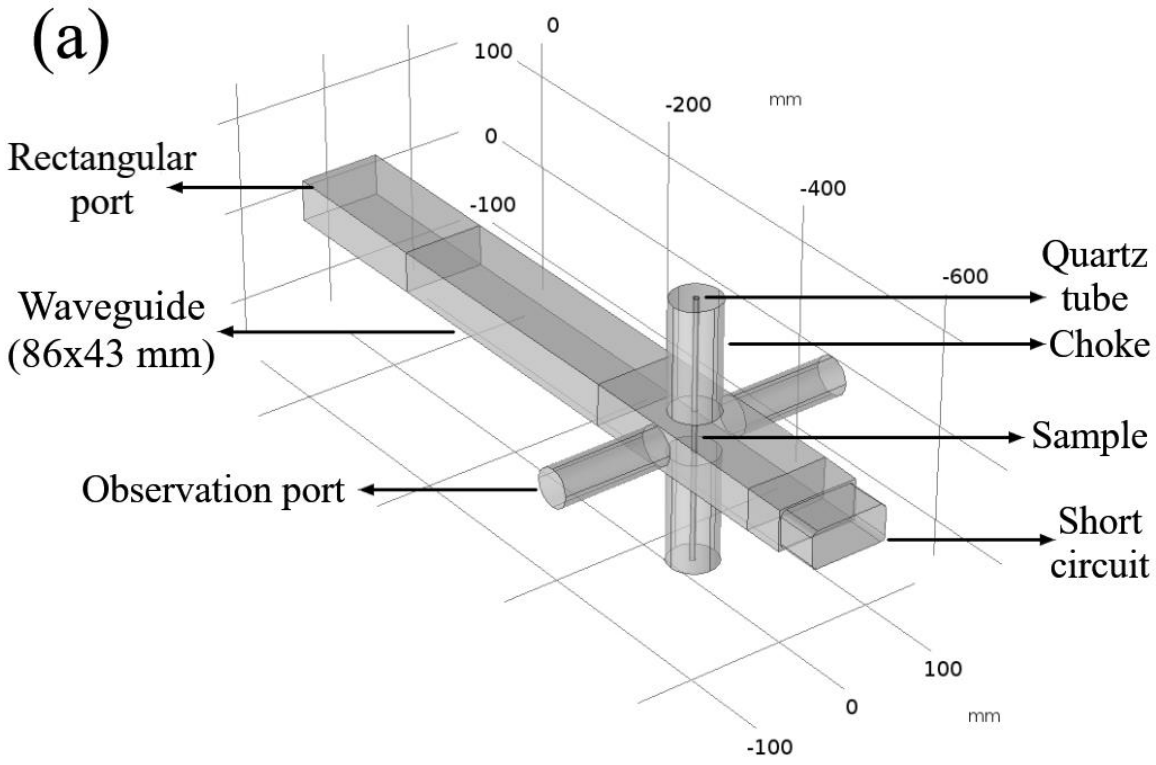

(b)

Electric field distribution

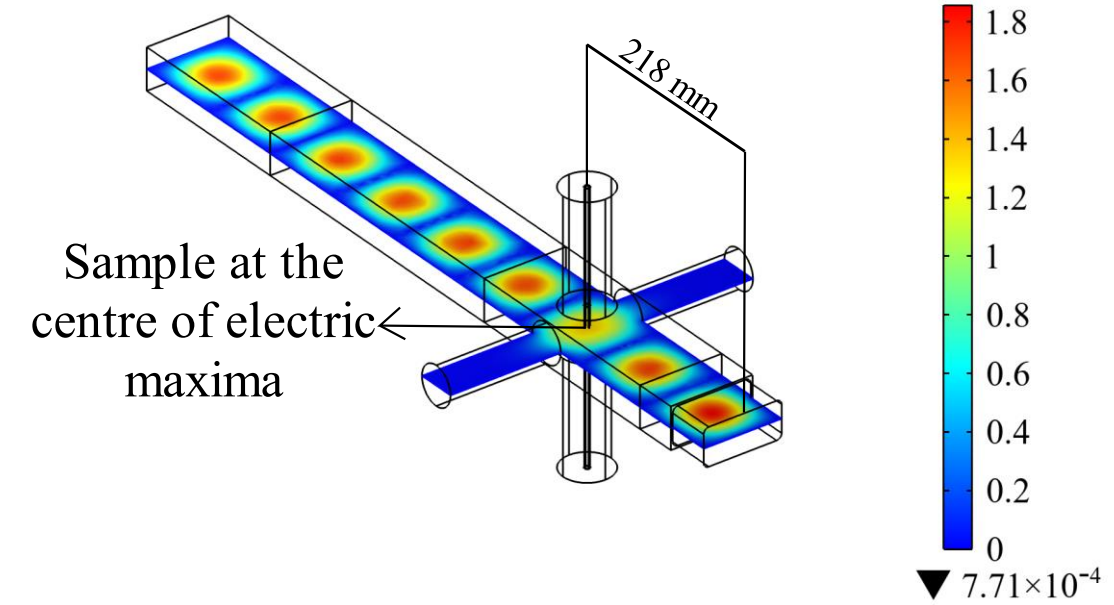

(c)

Magnetic field distribution

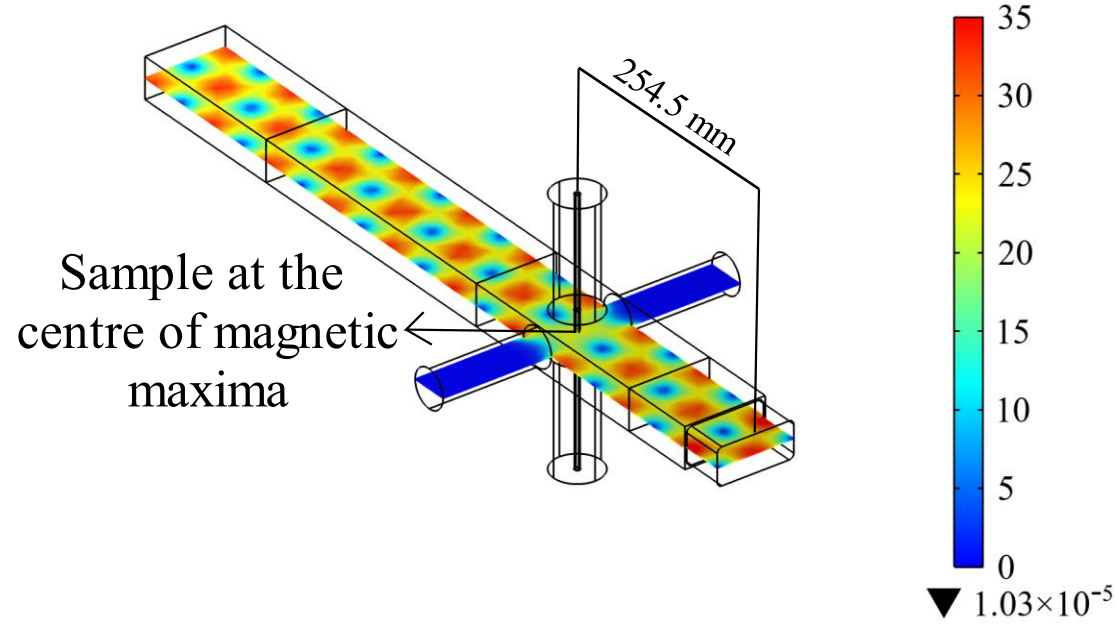

Figure 5. COMSOL Multiphysics simulation of the components of the heating setup (a) and the distribution of the electric (b) and magnetic (c) microwave fields at different short circuit positions at a power level of 130 W.

The maximum field intensity (either electric or magnetic) passing through the sample relies principally on the distance between the sample and the short circuit. The shifts in the short circuit position in Figure 5 (b) and (c) were adapted in the experiment and based on this simulation the experimental heating behaviour was studied. In highly lossy materials (e.g., graphite) slight variation to short circuit shift was introduced (refer to supplementary material Table S1 for more details).

3.4 X-Ray Diffraction analysis

XRD analysis was carried out for solid samples after cavity perturbation measurements and also after electric and magnetic heating experiments. A Bruker D8 Advance with a LYNXEYE 2D detector and a Cu kα radiation source was used for this analysis. The instrument was operated at a current and voltage of 40 mA and 40 kV, respectively. Data interpretation was performed using QualX 2.0 software [48].

3.5 Laser diffraction analysis

The performance of microwave heating is known to be affected by the particle size of the material [49]. Hence, the particle sizes of the powders used in this work were measured and are presented in Table 1. Beckman Coulter LS13320MW laser diffraction analyser with Aqueous Liquid Module (ALM) was used for the measurements of the particle size.

4 Results and Discussion

4.1 Dielectric characterisation

The dielectric properties of ZnO, Fe_2O_3, and $ZnFe_2O_4$ are presented in Figure 6. The behaviour of the dielectric properties of ZnO, Fe_2O_3, and $ZnFe_2O_4$ is very similar. Both the dielectric constant and the loss factor remain at values close to those seen at room temperature until temperatures of 600 – 700 °C. Above these temperatures, a sharp increase is observed. The variations in the dielectric properties may be attributed to the effect of temperature on the crystal lattice and the polarisability of molecules. The increase in the dielectric constant may be assigned to the increase in the crystal lattice spacing at high temperatures [42]. Consequently, more electron cloud deformation can be achieved [42]. The increase in lattice spacing also grants the ions forming the crystal broader potentials and more movement becomes attainable [42].

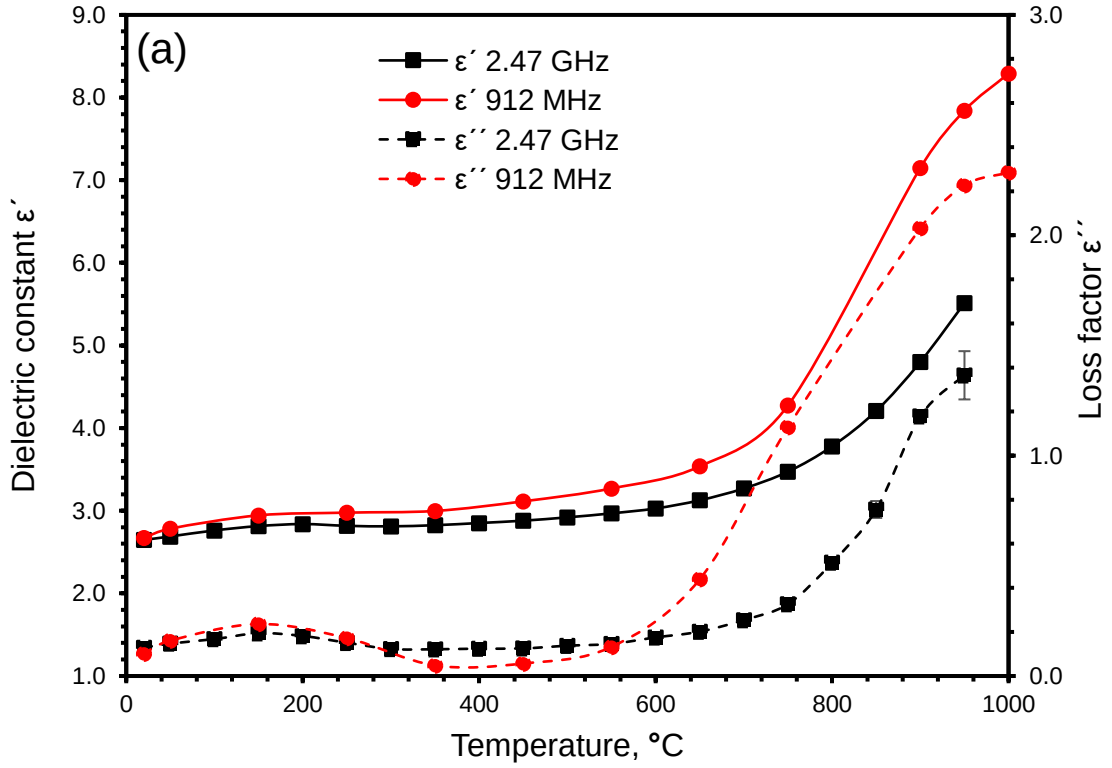

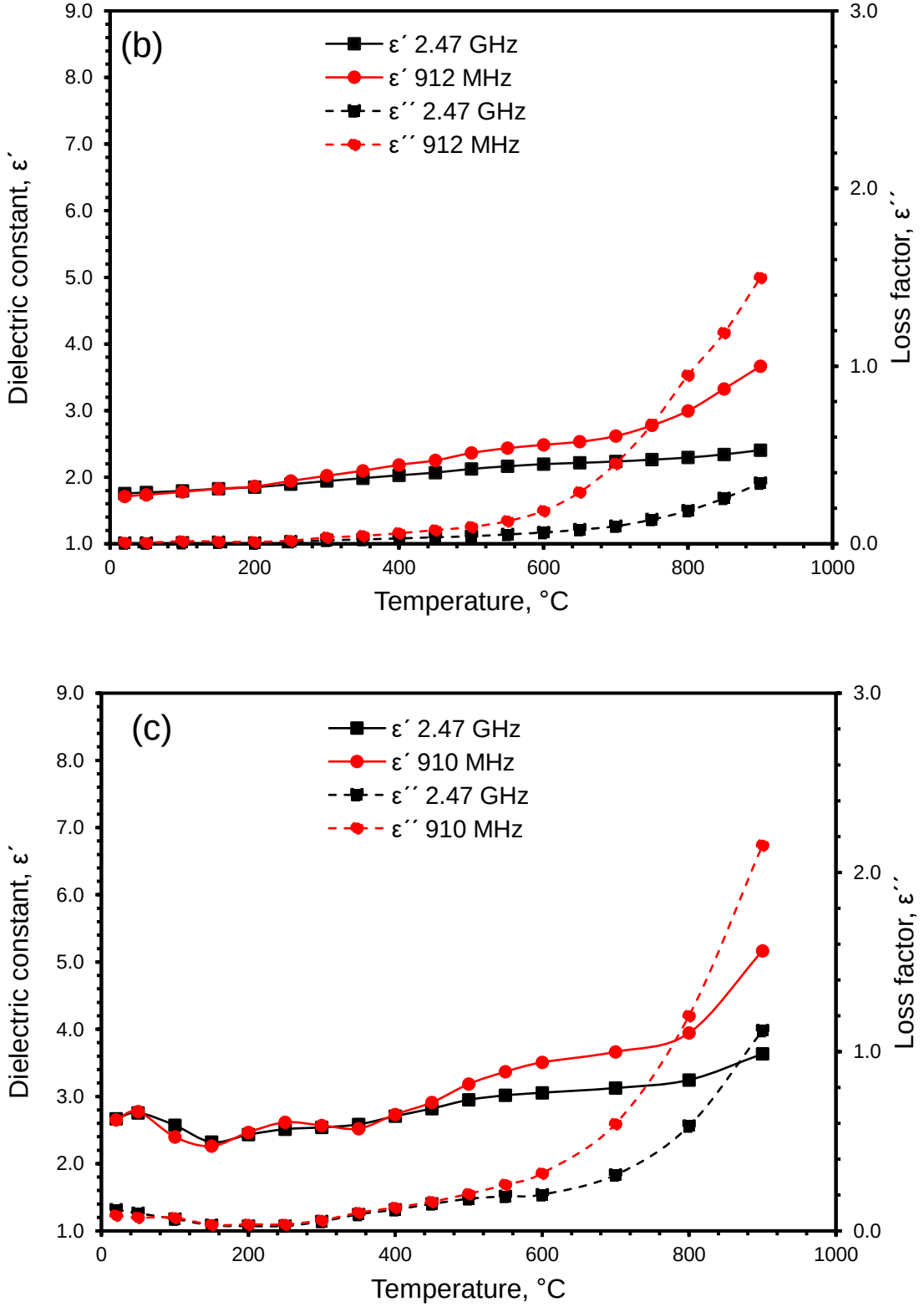

Figure 6. Dielectric properties profiles as a function of temperature at frequencies of 2.47 GHz and 912/910 MHz for (a) ZnO with a density of 1.89 g/cm^3, (b) Fe_2O_3 with a density of 0.58 g/cm^3 and (c) $ZnFe_2O_4$ with density of 1.09 g/cm^3.

The behaviour seen in Figure 6, can be understood by considering the effect of temperature on the relaxation time of dipoles in the sample. A relaxation time is defined as the time needed for a dipole to change orientation from one equilibrium position to another. For that, the potential double well theorem [34] was used in which the relaxation time τ_o is related to an activation energy U_a [34]. This activation energy resembles the energy barrier that must be overcome in order to polarise a dipole from one equiprobable position to another in materials where the intermolecular interactions are significant (e.g., solids). The relation is written as follows [34]:

$$\tau_o = \frac{e^{\frac{U_a}{k_b T}}}{\nu}\left[\frac{\varepsilon_s+2}{\varepsilon_\infty+2}\right] \quad (8)$$

Where, k_b is Boltzmann constant, T is absolute temperature, 1/ν is the time for a single oscillation in the potential well, and ε_s and ε_∞ are dielectric constant at static and very high frequency, respectively. In Equation 8, increasing the temperature, lowers the value of the term "$\frac{U_a}{k_b T}$" which decreases the relaxation time. As the relaxation time drops, more molecules are able to follow the rapid electric field oscillations, thus enhancing the extent of polarisation, which in turn, increases the value of the dielectric constant.

Table 1: Particle size of the powders used in this work.

Material	Mean particle size[a], µm
ZnO	466.2 ± 25.4
$ZnFe_2O_4$	13.2 ± 4.2
Fe_2O_3	36.6 ± 4.8
Fe_3O_4	31.7 ± 5.0
SiO_2	224.5 ± 7.6
PbO	101.1 ± 6.7
$CaCO_3$	3.3 ± 0.05
Graphite	60.8 ± 1.1

a: Mean ± SD.

The loss factor, in contrast, increases with a sharper slope. Such behaviour is attributed to the increase in the electrical conductivity at high temperatures [42]. The loss factor presented in Figure 6 is the "effective loss factor" which lumps the contribution from different microwave-matter interaction phenomena which in our case may be given as:

$$\varepsilon''_{effective} = \overbrace{\varepsilon''_{conduction}}^{1} + \overbrace{\varepsilon''_{polarisation}}^{2} \quad (9)$$

Where term 1 represents the contribution of electrical conductivity to the loss factor, while term 2 represents the contribution of dipolar polarisation. When crystalline solids are heated to high temperatures, lattice defects are formed under the action of thermal excitation which results in the formation of vacancies through which ionic conduction occurs under the influence of an external electric field [50]. Thus, the increase in the effective loss factor is mainly attributed to the increase in the conduction loss factor due to the increase in electrical conductivity at high temperatures (Equation 5). This point can further be emphasised by understanding the behaviour of the loss factor at different frequencies. At temperatures above 700 °C, the loss factor at 912/910 MHz is always greater than that at 2.47 GHz as seen in Figure 6. This is attributed to the inverse dependency of the conduction loss factor on the frequency of the radiation (Equation 5). The large difference in loss factor between 2.47 GHz and 912/910 MHz is only clearly seen at high temperatures where the electrical conduction contribution to the loss factor becomes significant. Since ZnO and $ZnFe_2O_4$ have relatively high loss factor at room temperature, dipolar polarisation might be assigned as the heating mechanism initially, followed by conduction loss at high temperatures.

Figure 7 represents the dielectric properties for PbO, SiO_2, and $CaCO_3$. The dielectric constant increases steadily from room temperature for all of them. The transformation of $CaCO_3$ into CaO in the temperature range 600 – 700 °C did not affect either the dielectric constant or the loss factor. PbO, on the other hand, shows a slight increase in the slope of the dielectric constant and loss factor at 650 °C which maybe regarded to the softening of the material (melting point is 888 °C). In general, however, the loss factor for all these materials does not show any significant increase and remains very close to zero at all temperatures. Comparing the data in Figures 7 and 6, it can be concluded that PbO, SiO_2, and $CaCO_3$ are expected to make the lowest contribution to the overall microwave heating of EAFD, while both ZnO and $ZnFe_2O_4$ can be classified as part of the major contributors to bulk heating. Fe_2O_3 might start contributing significantly to heating at temperatures above 600 °C.

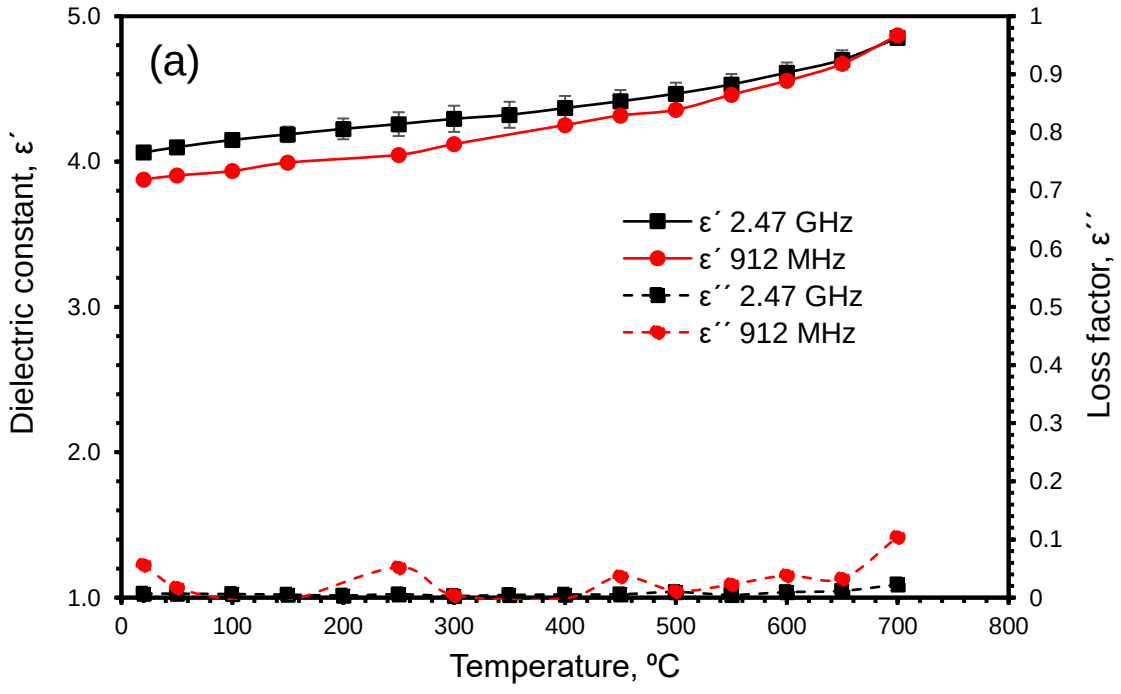

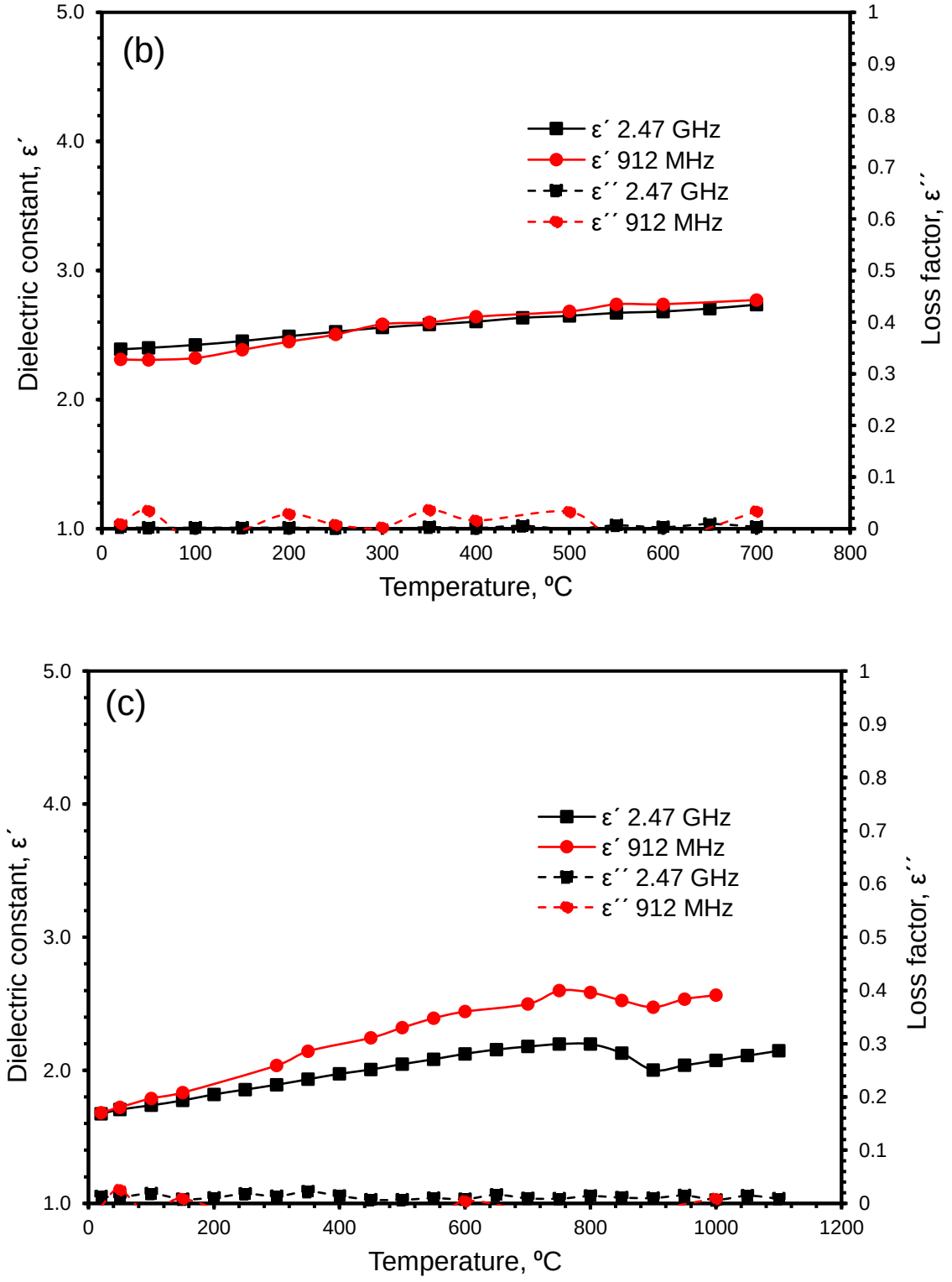

Figure 7. Dielectric properties profiles as a function of temperature at frequencies of 2.47 GHz and 912 MHz for (a) PbO with a density of 3.55 g/cm^3, (b) SiO_2 with a density of 1.50 g/cm^3 and (c) $CaCO_3$ with density of 0.50 g/cm^3.

Figure 8 shows the dielectric properties of Fe_3O_4 as a function of temperature at frequencies of 2.47 GHz and 910 MHz. The dielectric constant and the loss factor profiles show a unique behaviour for a solid since they follow the Debye theory of relaxation. The only difference is that Figure 8 shows the dielectric properties against temperature rather than frequency. The theory suggested by Debye, however, should still hold based on the qualitative shape of the curve and quantitative data obtained from it. At low temperatures, the material has a high relaxation time, which prohibits any form of polarisation thus yielding relatively low dielectric constant and loss factor. As the temperature increases (~ 100 °C), polarisation commences, leading to an increase in both the dielectric constant and the loss factor. With further temperature increase (~300 °C), the relaxation time becomes very short, and the polarisation vector stops lagging the electric field. At that point, the loss factor drops and the dielectric constant plateaus. Quantitatively, substituting the values of ε_s and ε_∞ (Figure 8) in the following equation: $\varepsilon^{''}_{max} = \frac{\varepsilon_s - \varepsilon_\infty}{2}$ which is extracted from Debye model, produces theoretical maximum loss factor values very close to those reported from the experiment; theoretical values are 2.53 and 2.24, while experimental values (Figure 8) are 2.56 and 2.15 at 2.47 GHz and 910 MHz, respectively. The relatively high loss factor seen for Fe_3O_4 compared with other EAFD constituents might be explained by the relatively high dc electrical conductivity reported in Miles et al. [51] for the material. This suggests that heating of Fe_3O_4 in the electric field can be attributed to dipolar polarisation and conduction loss mechanisms simultaneously and a maximum heating rate should be expected to be around 150 and 200 °C at frequencies of 910 MHz and 2.47 GHz, respectively.

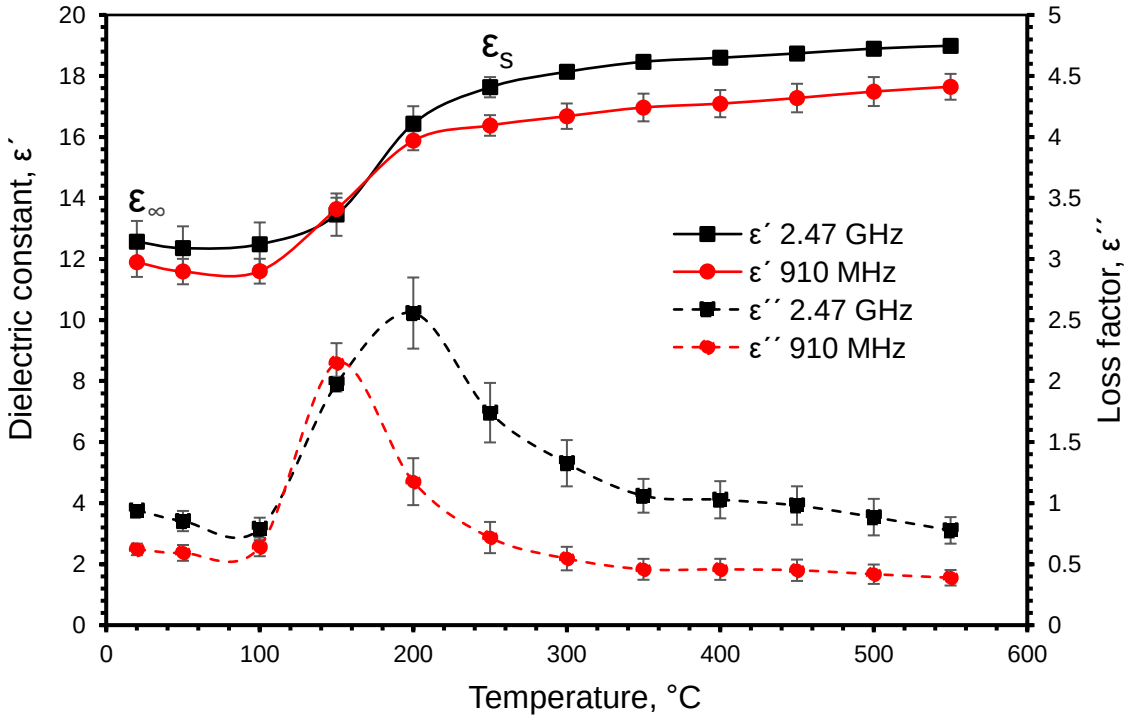

Figure 8. Dielectric properties profiles as a function of temperature for Fe_3O_4 at frequencies of 2.47 GHz and 910 MHz and a bulk density of 1.01 ± 0.012 g/cm^3.

4.2 Microwave electric and magnetic heating

Table 2 shows the heating rates and temperatures of EAFD constituents when exposed to pure electric and magnetic microwave fields at a frequency of 2.47 GHz and a power input of 118 ± 12 W. Heating profiles are in Figure S3 in the supplementary material.

Table 2: Microwave heating under the influence of pure electric and magnetic microwave fields at a frequency of 2.47 GHz and a power input of 118 ± 12 W.

Material	Electric Field			Magnetic Field		
	Heating rate °C/s [a]	Heating time, s	Temperature, °C	Heating rate °C/s [a]	Heating time, s	Temperature, °C
ZnO	37.1	30	846	No heating	No heating	No heating
$ZnFe_2O_4$	16.8	40	720	No heating	No heating	No heating
Fe_2O_3	1.65	210	180	No heating	No heating	No heating
Fe_3O_4	10.8	70	374	16.5	70	506

PbO	0.20	360	50	No heating	No heating	No heating
SiO_2	0.43	360	51	No heating	No heating	No heating
$CaCO_3$	2.31	150	168	No heating	No heating	No heating
C (graphite)	46.2	30	1026	18.2	70	560

a: Heating rate at first 20 seconds of heating.

The major contributors to the heating of EAFD are ZnO, $ZnFe_2O_4$, Fe_3O_4, and graphite having heating rates of 37.1, 16.8, 10.8, and 46.2 °C/s when heated in the electric field. Such result is directly related to their high loss factors reported earlier (Figures 6 and 8). This result also agrees with the high dielectric properties ($\varepsilon' = 26$ and $\varepsilon'' = 11$) reported for graphite in Hotta et al. [52]. PbO, SiO_2, $CaCO_3$, and Fe_2O_3 all exhibited very low heating rates and final temperatures (especially PbO and SiO_2) which is in agreement with the low loss factor values determined for these materials (Figures 6 and 7), rendering them the poorest contributors to EAFD microwave heating.

The most important feature in Table 2, however, is the distinctive response of Fe_3O_4 and graphite to the microwave magnetic field. Both Fe_3O_4 and graphite showed high heating rates of 16.5 and 18.2 °C/s, respectively, in the magnetic field, while the other constituents did not heat at all. This behaviour is attributed to the magnetic and electrically conductive nature of Fe_3O_4 and graphite, respectively. Heating of Fe_3O_4 can be attributed to magnetic hysteresis loss mechanism up to the curie temperature, while heating of graphite can be assigned to eddy currents formed in alternating magnetic fields. An attempt was made to heat Fe_3O_4 above its curie temperature (580 °C) by setting the microwave generator to its highest power output of 155 ± 12 W. A temperature of 594 °C was achieved in 60 s and up to 606 °C in 180 s; both are above the curie point. Despite the loss of magnetism of Fe_3O_4

at 580 °C, the sample was able to be heated 26 °C above its curie temperature. This behaviour might be explained by the relatively high electrical conductivity of Fe_3O_4 since the material has a band gap of 0.1 eV [53]. With such a small energy barrier between valence and conduction bands, significant electrical currents might form in the sample when exposed to external alternating magnetic fields. Exceeding the curie temperature might thus be assigned to the formation of eddy currents in the sample which causes Joule heating.

4.3 Magnetic heating and the selective extraction of Zn and Pb

In previous works, Al-Harahsheh et al. [19, 21] reported the significance of Fe_3O_4 elimination from EAFD on the selective extraction of zinc and lead upon the thermal treatment with halogenated plastics such as PVC and TBBPA. The elimination of Fe_3O_4 is meant to be through oxidising it to its higher oxidation state and more stable phase Fe_2O_3 [21]. The thermodynamics reported in these works provide a good insight to the spontaneity of chlorination/bromination of iron bearing compounds [19, 21]. Figure 9 shows the change in the Gibbs free energy of ZnO, PbO, Fe_3O_4, and Fe_2O_3 chlorination and the oxidation of Fe_3O_4 into Fe_2O_3 [21].

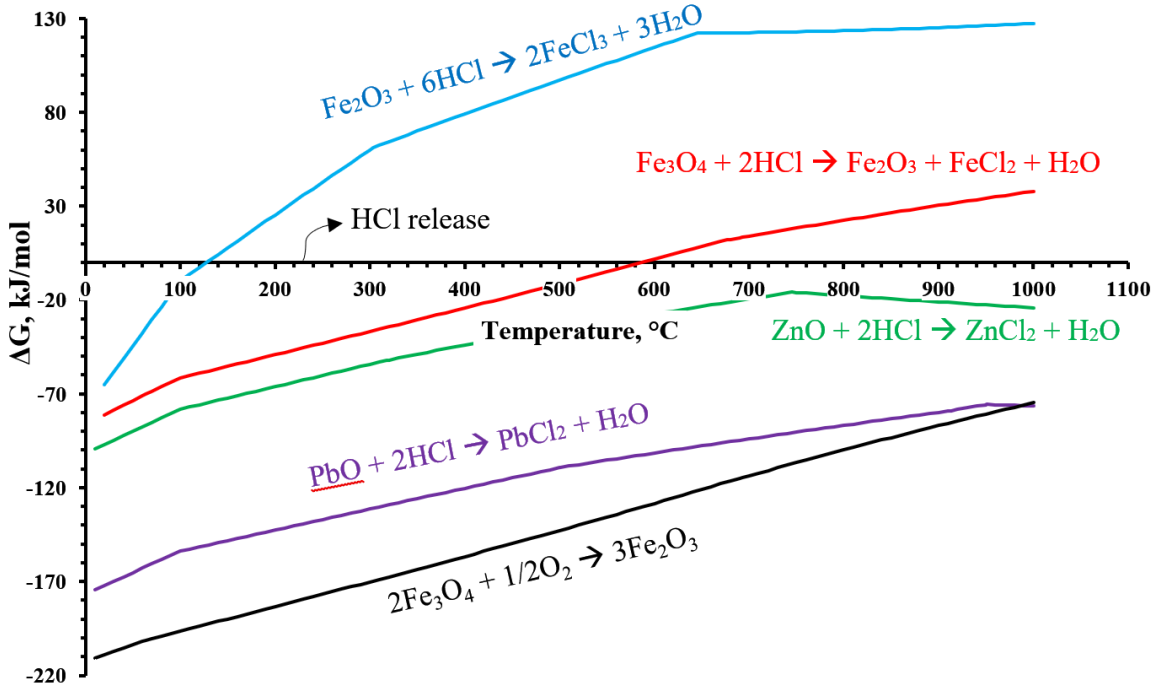

Figure 9. Change in Gibbs free energy of the main reactions of EAFD constituents with PVC decomposition product (HCl) using FACT SAGE software package [21].

The decomposition of PVC occurs at ~ 230 °C as reported in Al-Harahsheh et al. [2] after which approximately 58.3% of the polymer mass is transformed into gaseous HCl. The chlorination of both ZnO and PbO by HCl are thermodynamically favourable, resulting in the formation of water leachable chlorides ($ZnCl_2$ and $PbCl_2$). However, the chlorination of Fe_3O_4 is also thermodynamically possible in the temperature window 0 – 580 °C, yielding soluble $FeCl_2$ during water leaching step. To prevent the chlorination of Fe_3O_4, it must be oxidised to Fe_2O_3. Fe_2O_3 is impervious to chlorination and its reaction with HCl has ΔG values higher than zero above 120 °C. The kinetics of Fe_3O_4 oxidation, however, are known to be strongly temperature dependent [54, 55], such that increasing the temperature increases the reaction rate. Hence, efficient elimination of Fe_3O_4 can only be achieved at elevated temperatures. The utilisation of the microwave magnetic field allows targeting Fe_3O_4 alone without heating the other constituents. Fe_3O_4 can be heated selectively and oxidised efficiently (fast kinetics) to Fe_2O_3 prior to any polymer

decomposition into gaseous HCl. In contrast, using microwave electric field will heat up the entire EAFD-PVC mixture which causes the polymer to degrade before appreciable oxidation of Fe_3O_4 has taken place. This can negatively impact the extraction selectivity of other valuable metals such as zinc and lead.

The selective magnetic heating of Fe_3O_4 present in appreciable quantities in EAFD, in presence of O_2, will potentially contribute to more effective and sustainable recycling for this hazardous waste. Further investigation, however, is required to examine the implication of the reported results toward selective separation of zinc and lead from EAFD.

5 Conclusions

Dielectric characterisation and microwave heating of the main EAFD constituents in isolated electric and magnetic fields was carried out in this work. The main findings are the following:

- In the electric field maxima, ZnO, $ZnFe_2O_4$, Fe_3O_4, and graphite were found to be the main contributors to the microwave heating of EAFD, while Fe_2O_3, $CaCO_3$, SiO_2, and PbO were found to be the minor contributors to the overall heating (especially SiO_2 and PbO).
- The selective heating of Fe_3O_4 can be achieved by exposing it to a microwave magnetic field. Magnetic hysteresis loss mechanism is believed to be the source of heating up to the curie temperature (580 °C) above which eddy currents due to relatively high electrical conductivity are believed to be the source of heating.
- At temperatures above 600 °C, conduction loss becomes the dominant heating mechanism for the heating of ZnO, $ZnFe_2O_4$, and Fe_2O_3 as evident from their measured dielectric properties.

6 Acknowledgement

This work was supported by the Advanced Materials Research Group (AMRG)/Faculty of Engineering/University of Nottingham.

The authors would like to thank Teresa Needham from the Geography department at the University of Nottingham for conducting the particle size measurements.

References

1. Association, W.S., *Steel Facts. A collection of amazing facts about steel. Worldsteel*. 2018.
2. Al-Harahsheh, M., et al., *Pyrolysis of poly(vinyl chloride) and—electric arc furnacedust mixtures.* Journal of Hazardous Materials, 2015. **299**: p. 425-436.
3. Oustadakis, P., et al., *Hydrometallurgical process for zinc recovery from electric arc furnace dust (EAFD): Part I: Characterization and leaching by diluted sulphuric acid.* Journal of Hazardous Materials, 2010. **179**(1–3): p. 1-7.
4. Madias, J., *Electric Furnace Steelmaking*, in *Treatise on Process Metallurgy*. 2014. p. 271-300.
5. Xia, D. and C. Picklesi, *Microwave caustic leaching of electric arc furnace dust.* Minerals Engineering, 2000. **13**(1): p. 79-94.
6. Tsubouchi, N., et al., *Chemical characterization of dust particles recovered from bag filters of electric arc furnaces for steelmaking: Some factors influencing the formation of hexachlorobenzene.* Journal of hazardous materials, 2010. **183**(1-3): p. 116-124.
7. Montenegro, V., et al., *Hydrometallurgical treatment of steelmaking electric arc furnace dusts (EAFD).* Metallurgical and Materials Transactions B, 2013. **44**(5): p. 1058-1069.
8. Al-Harahsheh, M., et al., *Leaching of valuable metals from electric arc furnace dust—Tetrabromobisphenol A pyrolysis residues.* Journal of Analytical and Applied Pyrolysis, 2017. **125**: p. 50-60.
9. Havlik, T., et al., *Atmospheric leaching of EAF dust with diluted sulphuric acid.* Hydrometallurgy, 2005. **77**(1–2): p. 41-50.
10. Dutra, A.J.B., P.R.P. Paiva, and L.M. Tavares, *Alkaline leaching of zinc from electric arc furnace steel dust.* Minerals Engineering, 2006. **19**(5): p. 478-485.
11. Al-Makhadmeh, L.A., et al., *The Effectiveness of Zn Leaching from EAFD Using Caustic Soda.* Water, Air, & Soil Pollution, 2018. **229**(2): p. 33.
12. Teo, Y.Y., et al., *Hydrometallurgical extraction of zinc and iron from electric arc furnace dust (EAFD) using hydrochloric acid.* Journal of Physical Science, 2018. **29**: p. 49-54.
13. Morcali, M., et al., *Carbothermic reduction of electric arc furnace dust and calcination of waelz oxide by semi-pilot scale rotary furnace.* Journal of Mining and Metallurgy B: Metallurgy, 2012. **48**(2): p. 173-184.
14. Suetens, T., et al., *Comparison of electric arc furnace dust treatment technologies using exergy efficiency.* Journal of cleaner production, 2014. **65**: p. 152-167.
15. Lee, G.-S. and Y.J. Song, *Recycling EAF dust by heat treatment with PVC.* Minerals engineering, 2007. **20**(8): p. 739-746.
16. Al-harahsheh, M., et al., *Microwave treatment of electric arc furnace dust with PVC: Dielectric characterization and pyrolysis-leaching.* Journal of Hazardous Materials, 2014. **274**: p. 87-97.
17. Al-harahsheh, M., S. Kingman, and I. Hamilton, *Microwave treatment of electric arc furnace dust with Tetrabromobisphenol A: Dielectric characterization and pyrolysis-leaching.* Journal of Analytical and Applied Pyrolysis, 2017. **128**: p. 168-175.

18. Al-Harahsheh, M., et al., *Treatments of electric arc furnace dust and halogenated plastic wastes: A review.* Journal of Environmental Chemical Engineering, 2018: p. 102856.
19. Al-Harahsheh, M. and M. Altarawneh, *Thermodynamic analysis on the oxidative pyrolytic treatment of electric arc furnace Dust–TBBA blends.* Oxidation of Metals, 2018: p. 1-28.
20. Al-Harahsheh, M., et al., *Bromine fixing ability of electric arc furnace dust during thermal degradation of tetrabromobisphenol: Experimental and thermodynamic analysis study.* Journal of analytical and applied pyrolysis, 2018. **134**: p. 503-509.
21. Al-Harahsheh, M., *Thermodynamic Analysis on the Thermal Treatment of Electric Arc Furnace Dust-PVC Blends.* Arabian Journal for Science and Engineering, 2017: p. 1-13.
22. Sun, X., J.-Y. Hwang, and X. Huang, *The microwave processing of electric arc furnace dust.* Jom, 2008. **60**(10): p. 35-39.
23. Zhou, Y., et al., *Separation of ZnO from the stainless steelmaking dust and graphite mixture by microwave irradiation.* High Temperature Materials and Processes, 2015. **34**(2): p. 177-184.
24. Omran, M., et al., *Dielectric properties and carbothermic reduction of zinc oxide and zinc ferrite by microwave heating.* Royal Society Open Science, 2017. **4**(9): p. 170710.
25. Omran, M., T. Fabritius, and E.-P. Heikkinen, *Selective Zinc Removal from Electric Arc Furnace (EAF) Dust by Using Microwave Heating.* Journal of Sustainable Metallurgy, 2019. **5**(3): p. 331-340.
26. Ye, Q., et al., *Microwave-assisted reduction of electric arc furnace dust with biochar: an examination of transition of heating mechanism.* ACS Sustainable Chemistry & Engineering, 2019. **7**(10): p. 9515-9524.
27. Ye, Q., et al., *Microwave-assisted self-reduction of EAF dust-biochar composite briquettes for production of direct reduced iron.* Powder Technology, 2020. **362**: p. 781-789.
28. Ye, Q., et al., *Microwave-assisted reduction of electric arc furnace dust with biochar: an examination of transition of heating mechanism.* ACS Sustainable Chemistry & Engineering, 2019.
29. Cruells, M., A. Roca, and C. Núñez, *Electric arc furnace flue dusts: characterization and leaching with sulphuric acid.* Hydrometallurgy, 1992. **31**(3): p. 213-231.
30. Sekula, R., et al., *Electric arc furnace dust treatment: investigation on mechanical and magnetic separation methods.* Waste management & research, 2001. **19**(4): p. 271-275.
31. Sofilić, T., et al., *Characterization of steel mill electric-arc furnace dust.* Journal of Hazardous Materials, 2004. **109**(1–3): p. 59-70.
32. de Vargas, A.S., Â.B. Masuero, and A.C. Vilela, *Investigations on the use of electric-arc furnace dust (EAFD) in Pozzolan-modified Portland cement I (MP) pastes.* Cement and Concrete research, 2006. **36**(10): p. 1833-1841.
33. Sun, J., W. Wang, and Q. Yue, *Review on microwave-matter interaction fundamentals and efficient microwave-associated heating strategies.* Materials, 2016. **9**(4): p. 231.

34. Metaxas, A.a. and R.J. Meredith, *Industrial microwave heating*. 1983: IET.
35. Galema, S.A., *Microwave chemistry.* Chemical Society Reviews, 1997. **26**(3): p. 233-238.
36. Thostenson, E. and T.-W. Chou, *Microwave processing: fundamentals and applications.* Composites Part A: Applied Science and Manufacturing, 1999. **30**(9): p. 1055-1071.
37. Kingman, S., *Recent developments in microwave processing of minerals.* International materials reviews, 2006. **51**(1): p. 1-12.
38. Rosa, R., P. Veronesi, and C. Leonelli, *A review on combustion synthesis intensification by means of microwave energy.* Chemical Engineering and Processing: Process Intensification, 2013. **71**: p. 2-18.
39. Haimbaugh, R., *Theory of heating by induction.* Practical Induction Heat Treating, 2001: p. 5-11.
40. Saini, S., et al., *Magnetism: a primer and review.* American Journal of Roentgenology, 1988. **150**(4): p. 735-743.
41. Van der Zaag, P., P. Van der Valk, and M.T. Rekveldt, *A domain size effect in the magnetic hysteresis of NiZn-ferrites.* Applied physics letters, 1996. **69**(19): p. 2927-2929.
42. Bobicki, E., et al., *High temperature permittivity measurements of selected industrially relevant ores: Review and analysis.* Minerals Engineering, 2020. **145**: p. 106055.
43. Gabriel, C., et al., *Dielectric parameters relevant to microwave dielectric heating.* Chemical Society Reviews, 1998. **27**(3): p. 213-224.
44. Al-Harahsheh, M. and S. Kingman, *Microwave-assisted leaching—a review.* Hydrometallurgy, 2004. **73**(3-4): p. 189-203.
45. Horikoshi, S., T. Sumi, and N. Serpone, *Unusual effect of the magnetic field component of the microwave radiation on aqueous electrolyte solutions.* Journal of Microwave Power and Electromagnetic Energy, 2012. **46**(4): p. 215-228.
46. Aguiar, P.M., J.-F. Jacquinot, and D. Sakellariou, *Experimental and numerical examination of eddy (Foucault) currents in rotating micro-coils: Generation of heat and its impact on sample temperature.* Journal of Magnetic Resonance, 2009. **200**(1): p. 6-14.
47. Al-Harahsheh, M., et al., *Dielectric properties of Jordanian oil shales.* Fuel Processing Technology, 2009. **90**(10): p. 1259-1264.
48. Altomare, A., et al., *QUALX2. 0: a qualitative phase analysis software using the freely available database POW_COD.* Journal of Applied Crystallography, 2015. **48**(2): p. 598-603.
49. Yoshikawa, N., E. Ishizuka, and S. Taniguchi, *Heating of metal particles in a single-mode microwave applicator.* Materials transactions, 2006. **47**(3): p. 898-902.
50. Jonscher, A.K., *Dielectric relaxation in solids.* Journal of Physics D: Applied Physics, 1999. **32**(14): p. R57.
51. Miles, P., W. Westphal, and A. Von Hippel, *Dielectric spectroscopy of ferromagnetic semiconductors.* Reviews of Modern Physics, 1957. **29**(3): p. 279.

52. Hotta, M., et al., *Complex permittivity of graphite, carbon black and coal powders in the ranges of X-band frequencies (8.2 to 12.4 GHz) and between 1 and 10 GHz.* ISIJ international, 2011. **51**(11): p. 1766-1772.
53. Cornell, R.M. and U. Schwertmann, *The iron oxides: structure, properties, reactions, occurrences and uses*. 2003: John Wiley & Sons.
54. Papanastassiou, D. and G. Bitsianes, *Mechanisms and kinetics underlying the oxidation of magnetite in the induration of iron ore pellets.* Metallurgical Transactions, 1973. **4**(2): p. 487-496.
55. Monazam, E.R., R.W. Breault, and R. Siriwardane, *Kinetics of Magnetite (Fe3O4) Oxidation to Hematite (Fe2O3) in Air for Chemical Looping Combustion.* Industrial & Engineering Chemistry Research, 2014. **53**(34): p. 13320-13328.